



TECHNICAL ARTICLE

Revealing the Dynamics of Helium Bubbles Using In Situ Techniques

SI-MIAN LIU,¹ SHI-HAO LI,^{1,2} and WEI-ZHONG HAN^{1,3}

1.—Center for Advancing Materials Performance from the Nanoscale, State Key Laboratory for Mechanical Behavior of Materials, Xi'an Jiaotong University, Xi'an 710049, China. 2.—School of Materials Science and Engineering, Zhengzhou University, Zhengzhou 450001, China. 3.—e-mail: wzhanxjtu@mail.xjtu.edu.cn

As one of the major irradiation defects, helium bubbles have a marked influence on the microstructures and mechanical properties of metals. In recent decades, many experiments and simulations have focused on helium bubbles to reveal their nucleation and growth mechanisms, dynamic evolution under stimulations, and their effects on mechanical properties. With the quick development of various in situ techniques, the abundant dynamic features of helium bubbles have been revealed. In this review, we briefly explore the related researches on the dynamic evolution of helium bubbles under simulated service conditions, such as at high temperatures, under irradiation, and upon mechanical loading. We also discuss the challenges and opportunities in revealing the dynamics of helium bubbles using in situ technologies. This short review intends to advance our understanding of the failure mechanisms of helium-irradiated metals and the basic properties of irradiation-induced helium bubbles.

INTRODUCTION

Helium ions, which can be produced by (n, α) nuclear reactions in fast breeder reactors and fusion devices or (p, α) reactions in cladding materials from spallation neutron sources, are prone to precipitate into bubbles because of their extremely low solubility in metals.^{1,2} Helium bubbles are typical radiation defects that can lead to swelling,^{3,4} hardening,⁵ blistering,⁶ and macroscopic embrittlement,^{7–9} all of which pose a significant threat to the stability and reliability of structural materials in reactors. For instance, the formation and coarsening of bubbles are critical processes in radiation swelling and surface blistering in metals.⁶ The growth and coalescence of helium bubbles along grain boundaries under elevated temperatures are the fundamental reason for high-temperature helium embrittlement, which is manifested as intergranular catastrophic failure.^{7–9} Metals and alloys serving in nuclear reactors experience thermal annealing, continuous particle irradiation, and mechanical loading; therefore, it is important to investigate the dynamics of helium bubbles under these service conditions.

In situ characterization techniques, which provide a direct, real-time view on microstructural evolution in materials, play an increasing important role in revealing the dynamics of helium bubbles under thermal annealing, irradiation, and mechanical loading. In the past decade, in situ techniques have been widely used to study the dynamics of helium bubbles, which provide abundant details and novel behaviors of them under various complicated service conditions.^{10–16} Figure 1 lists several typical sample geometries used in in situ experiments for studying the dynamics of helium bubbles.^{12–15} In situ nano-scale samples are fabricated by focused ion beams, and it is convenient to investigate the effect of helium bubbles on the mechanical behavior using transmission electronic microscopy (TEM). For micro-scale tensile samples, in situ mechanical tests can be performed using scanning electron microscopy.¹⁶ In addition, an in situ helium ion microscope has been used to study the blistering behavior on the surface of bulk tungsten under in situ helium implantation.¹⁷ In situ small-angle x-ray scattering has been adopted to reveal the bubble evolution (helium density and pressure) by analyzing the scattering profile

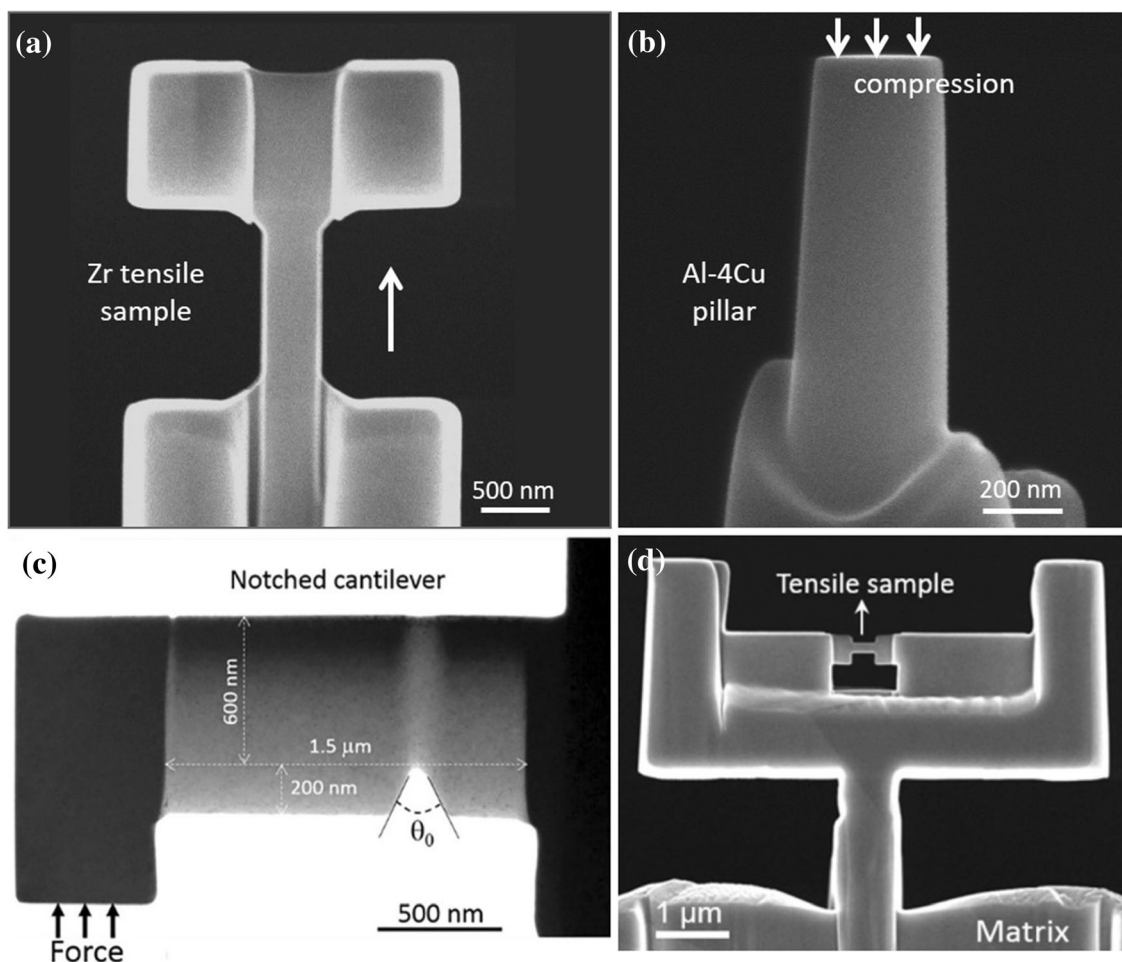


Fig. 1. Typical sample geometries used in in situ investigations. (a) Micro-scale tensile sample (reprinted with permission from Ref. 13); (b) nano-scale pillar for compression (reprinted with permission from Ref. 14); (c) notched cantilever for in situ cracking observation (reprinted with permission from Ref. 15); (d) PTP sample designed for high-resolution in situ microstructures observation (reprinted with permission from Ref. 12).

contributed by a large bubble population.¹⁸ Recently, three-dimensional mapping has been conducted to reveal the mechanism of bubble nucleation and growth.¹⁹

In this review, we briefly overview the dynamic evolution of helium bubbles under thermal annealing, irradiation, and mechanical loading in metals. The critical mechanisms responsible for helium bubble evolution in metals are summarized and discussed. Finally, we also discuss the challenges and opportunities in revealing the dynamics of helium bubbles using in situ technologies.

DYNAMIC EVOLUTION OF HELIUM BUBBLES UNDER STIMULATIONS

Dynamics of Helium Bubbles Under In Situ Annealing

In situ tests have demonstrated that the dynamics of helium bubbles under thermal annealing consist of bubble migration, coarsening, and disappearing.^{20–29} The evolution of helium bubbles differs

under various annealing temperatures and in different metals. Helium bubbles show random migration both in the interior of grains and along grain boundaries.^{21–25} Figure 2 shows an example of helium bubble migration and coalescence in the interior of a grain in Fe at 1023 K. The bubble indicated by an arrow moved from bottom to top (Fig. 2). At 151 s, the bubble coalesced with a larger one (Fig. 2c) and then disappeared at 154 s.²⁵ Similar migration behavior was also observed for helium bubbles along the grain boundary in Al at 833 K: bubble A-1 with a diameter of 2.6 nm migrated downwards along the grain boundary, while bubble A-2 with a diameter of 2.3 nm moved in the opposite direction along the same boundary (Fig. 2d–f).²² The mean square of the bubble migration distance is proportional to the annealing time, indicating a Brownian-type motion.^{21–25} The migration of helium bubbles along the grain boundary and interface can be accelerated compared with the grain interior.²⁰ The degree of acceleration depends on the boundary or phase interface's orientation

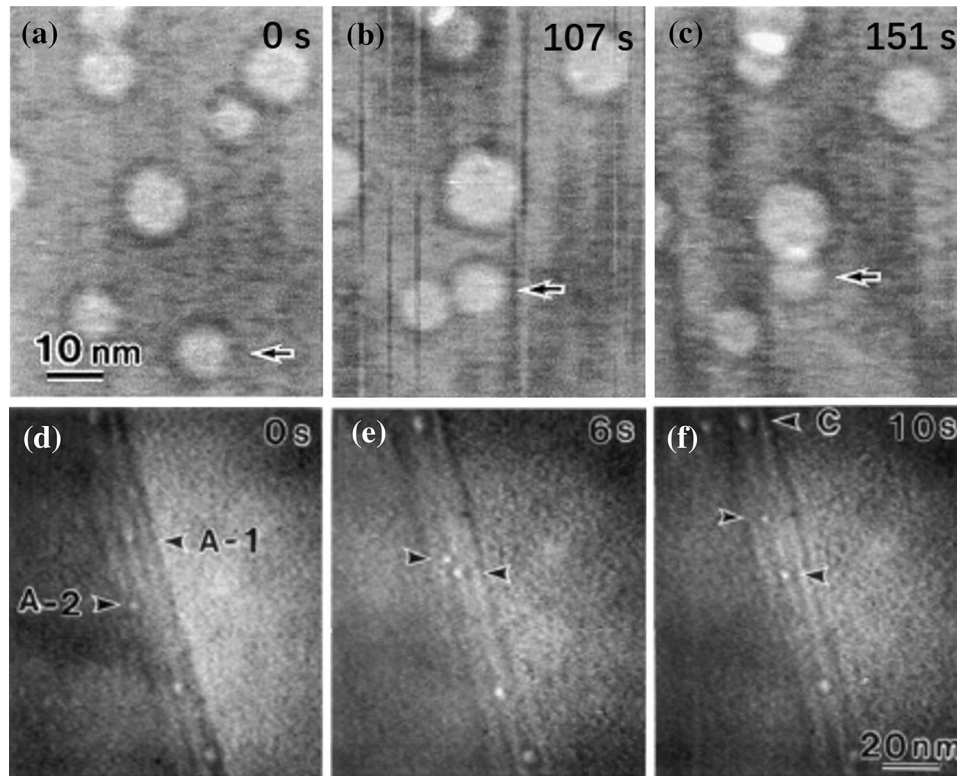


Fig. 2. (a)–(c) A sequence of images showing helium bubble motion inside a grain in Fe at 1023 K (reprinted with permission from Ref. 25). The arrowed bubble (diameter, 10 nm) moves toward to the larger one and merges into the larger bubble at 154 s. (d)–(f) A sequence of images showing helium bubble motion along a grain boundary in Al at 833 K (reprinted with permission from Ref. 22). Bubble A-1 (diameter, 2.6 nm) has moved downwards along the boundary, while bubble A-2 (diameter, 2.3 nm) has moved upwards along the boundary. Bubble A-2 finally coalesced with bubble C at 285 s.

relationship and atomic structures.^{24,25} During annealing, the bubble adjacent to the grain boundary first moved randomly, then fell into the grain boundary sink during the random movement, and finally moved rapidly along the boundary.²⁰ The bubble diffusivity reflects the mobility of helium bubbles and depends on the adjacent chemical composition, bubble size, bubble shape, and annealing temperature, among other factors.^{21–25} For instance, Cr segregation on the helium bubble surface decreases the bubble diffusivities because of the decrease in the surface diffusion of the helium bubbles.^{24,25} In addition, larger bubbles (> 15 nm) are hard to move, but helium bubbles with a size < 8 nm have high mobility.²⁹ In general, spherical helium bubbles migrate more easily and frequently than faceted helium bubbles because of the anchoring effect of sessile dislocations along the edges.³⁰ At lower temperatures, the dynamic motion of helium bubbles during annealing is not obvious because of their low bulk and surface diffusivity. Only those tiny helium bubbles with a diameter < 2 nm disappeared during annealing.²⁹

Two main well-known mechanisms, Ostwald ripening (OR) and migration and coarsening (MC), are responsible for bubble growth and coarsening.^{31–34} Previous characterization found that helium bubble coarsening is a common phenomenon

in the post-annealing of helium-irradiated samples.³⁵ By in situ observation during annealing, the variation of the bubble shape and size can be monitored; thus, the coarsening mechanism of the helium bubble can be captured. At 918 K, the smaller helium bubbles in Al move randomly, and once they touch the larger ones, they coalesce into one bubble within a couple of seconds.^{21,23} The main growth mechanism for faceted helium bubbles is MC, which depends on the diffusion of matrix atoms or ledge nucleation,³⁶ while OR is driven by the differences in the bubble pressure.²⁷ Both mechanisms were associated with the annealing temperature: i.e., MC preferred to occur at lower temperatures, while OR dominated at higher temperatures.³⁷ The in situ observation demonstrated that the size of the helium bubbles increased slowly with the elevation of temperatures < 923 K for a Zr-Sn-Nb-Fe-Cr alloy during in situ heating; however, the size of the helium bubbles evolved dramatically once above this critical temperature,³⁸ which resulted from a different coarsening mechanism. The coarsening of helium bubbles inside a grain is always dominated by bubble coalescence; however, the coarsening process of helium bubbles at grain boundaries behaved like a pancake²⁸ (Fig. 3). A neck is produced when two bubble tips contact each other., and the underlying mechanism

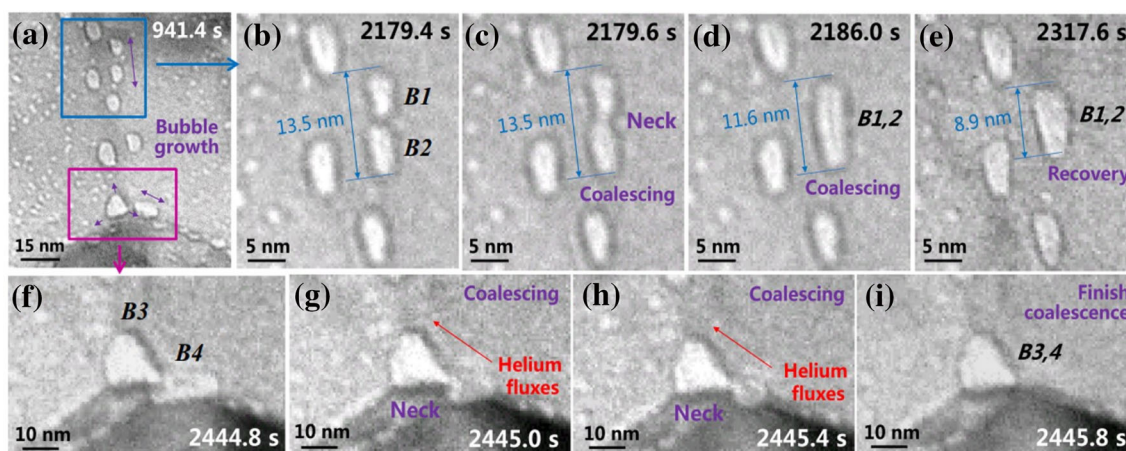


Fig. 3. Sequence of snapshots showing the dynamical growth and coalescence of intergranular helium bubbles (reprinted with permission from Ref. 28). (a) Bubble growth along grain boundaries as indicated by the arrows after heating for 941.4 s at 400°C; (b) further growth and touching of bubbles B1; (c)–(e) coalescence of B1 and B2; (f)–(i) growth and coalescence of B3 and B4 located at the grain boundary triple junction.

of the pancake shaped evolution in the growth process is mediated by the coupling of the metal matrix interface diffusion and non-zero grain boundary fluxes.²⁸ The coarsening by larger bubbles swallowing smaller bubbles can also be observed because of the pressure gradient between the two bubbles (Fig. 3).

Dynamics of Helium Bubbles Under In Situ Irradiation

Helium bubbles undergo migration, coalescence, coarsening, and shrinkage under in situ irradiation. However, the underlying mechanisms differ from that of helium bubbles under thermal annealing.^{39–41} Due to high-energy ion irradiation, bubble coalescence occurs as a result of the net displacement of matrix atoms out of the volume between two bubbles or as a result of the cascade-induced migration of the bubbles.^{42,43} Helium bubbles also displayed Brownian motion under high-energy ion beam irradiation.^{39–41} The bubble motion at higher-temperature annealing is driven by thermal motion, which is far larger than the thermal spike effects caused by cascades.³⁰ The demonstrated mobility of helium bubbles increased or decreased under in situ irradiation.^{30,39–41} The retardation of helium bubble migration was associated with the increasing of bubble diameter because of the incorporation of excess vacancies under in situ irradiation.^{21–23} In contrast, there are three main reasons for the acceleration of bubble movement under in situ irradiation. First, irradiation introduces profuse point defects, dislocation lines, and dislocation loops. Helium bubbles on those defects may preferentially absorb self-interstitial atoms, resulting in an increase in the internal pressure, which makes them spherical.³⁹ These spherical bubbles move more easily and faster at lower temperatures than the non-spherical bubbles.^{29,30} This mechanism can also explain the observation of intermittent bubble

motion along dislocation lines or loops.^{30,39–41} Second, a chemical gradient is produced near a dislocation loop or line due to different concentrations of point defects, which causes bubble motion.⁴¹ Third, irradiation changes the migration of helium bubbles from Brownian motion to a long-distance rectilinear motion. Figure 4 shows the rapid motion of a helium bubble across 10 nm under in situ irradiation (marked by a white arrow).⁴¹ This kind of rapid motion has nothing to do with bubble sizes. The helium bubbles only had random motion under the beam-off condition, while showing a rapid long-distance rectilinear motion under in situ irradiation.^{39–41} Helium bubbles near the specimen surface or away from the cascade-rich region shrink by the absorption of the interstitial atoms produced by irradiation.⁴⁴ In addition, the helium atoms in the bubble are likely to be knocked out by a direct collision, which is accompanied by the emission of vacancies.^{30,44} The retrapping of the emitted vacancies and helium atoms formed into small satellite bubbles close to the original larger bubbles.⁴³

Dynamics of Helium Bubbles Under In Situ Mechanical Loading

The helium bubbles demonstrate migration, coarsening, elongation, and cleavage under mechanical loading.^{10–12,45–48} Generally, the migration of helium bubbles under mechanical loading is driven by stress gradients, such as around the crack tip, grain boundary, or in a strain-localized region.⁴⁷ In addition, helium bubbles with sizes of 20–40 nm can be dragged by moving dislocations.⁴⁵ When driven by the stress gradient, the bubble diameter increases through bubble migration and coalescence as well as the absorption vacancies induced by dislocation slips and their interactions. In the coalescence processes, neighboring bubbles with similar sizes can coalesce into a long bubble, which further becomes spherical with the assistance of

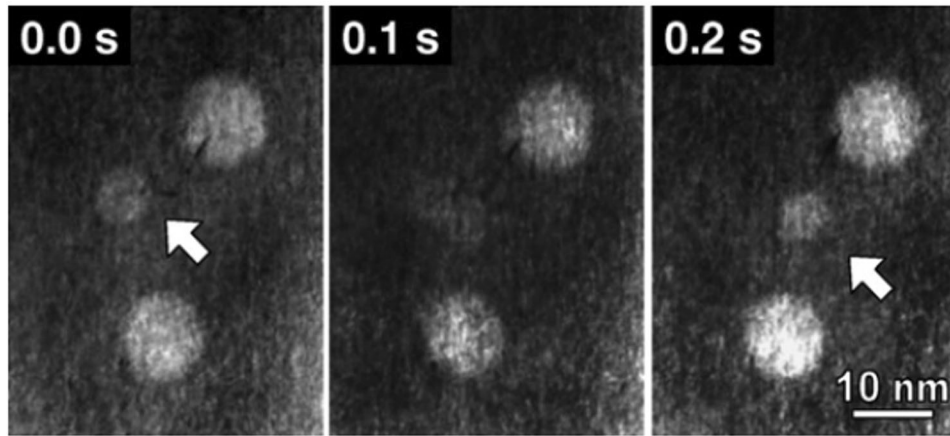


Fig. 4. A series of video frames showing the motion of helium bubbles in Cu under 400 keV Cu⁺ irradiation at 823 K (reprinted with permission from Ref. 41).

local internal surface diffusion.⁴⁸ This results in a decrease in the helium bubble density and an increase in their spacing, which suppresses further coalescence of the bubbles and reduces the bubble-coarsening rate.^{18,47}

Localized deformation has been demonstrated to significantly enhance bubble coarsening, followed by bubble elongation and cleavage.^{10–12} Figure 5 presents snapshots that record the bubble elongation and cleavage under mechanical loading. With increasing strain, the helium bubbles elongated nearly along the loading direction and formed into a rod-like shape with a high aspect ratio.¹² The spherical bubbles that evolved into cylinder-shaped bubbles were also observed in helium-irradiated Al foils.¹¹ With further localization and necking deformation, the helium bubbles were stretched into dumbbell shapes. By dislocation cutting or Rayleigh instability-controlled processes, the elongated helium bubbles split into several small helium bubbles.^{10–12} Similar helium bubble cleavage was also observed in helium-irradiated Al-4Cu.¹¹ Upon tension, the equilibrium pressure of helium bubbles $P = 2\gamma/r$ decreases as a result of stress-induced vacancy absorption and bubble size growth.⁴⁹ The elongated bubbles with low internal pressure are cut through more easily by dislocations. In addition, the foil sample used in TEM became thinner and thinner, which led to the transformation of large helium bubbles into cracks or surface flaws in the stress-concentration region.^{45–48}

EFFECT OF HELIUM BUBBLES ON PLASTIC DEFORMATION

Extensive experimental and modeling studies have focused on the effects of helium bubbles on the mechanical behaviors of metals.^{50–52} Dislocation gliding and deformation twinning are two of the main mechanisms mediating the plasticity of metals. Bubble–dislocation interactions and bubble–twin interactions can dramatically alter the

deformation mode of metals and alloys. In situ nano-mechanical testing provides a powerful method for shedding light on the dynamic mechanism of helium bubbles on the plastic deformation in irradiated metals.

Helium Bubbles as Internal Dislocation Sources and Obstacles

During plastic deformation, helium bubbles in submicron-scale metals (Cu, Al-4Cu, and Zr) play the role of internal dislocation sources, which promote dislocation nucleation instead of only depending on surface sources.^{10–13} In addition, helium bubbles also serve as shearable obstacles, impede full dislocation motion, and promote dislocation–dislocation interactions. Therefore, they reduce the dislocation mean free path and the dislocation mobility, which increases dislocation storage and leads to strong strain-hardening, high flow stress, and stable deformation in small-volume metals.^{10–13,52–55}

The unique roles of helium bubbles in deformation also promote the recovery of super-elasticity in small-volume shape memory alloys.^{56–58} Under the strain of the shape memory alloy pillar, radiation-induced helium bubbles play the role of martensite nucleation sites.⁵⁶ Furthermore, many helium bubbles create a large area of internal surface inside a small-volume pillar, which compensates for the surface-energy contribution to the total free energy of the martensitic phase transformation. In addition, the pressurized helium bubbles are strong obstacles for dislocation slips; therefore, they stop shear localization and avoid the earlier failure of the sample. Due to the combined roles of helium bubbles described above, the helium-irradiated small-volume shape memory alloys still possess excellent super-elasticity.⁵⁶

Helium bubbles also assist in detwinning due to the strong dislocation–bubble interaction producing back stress.⁵⁹ Successive Shockley partial emissions

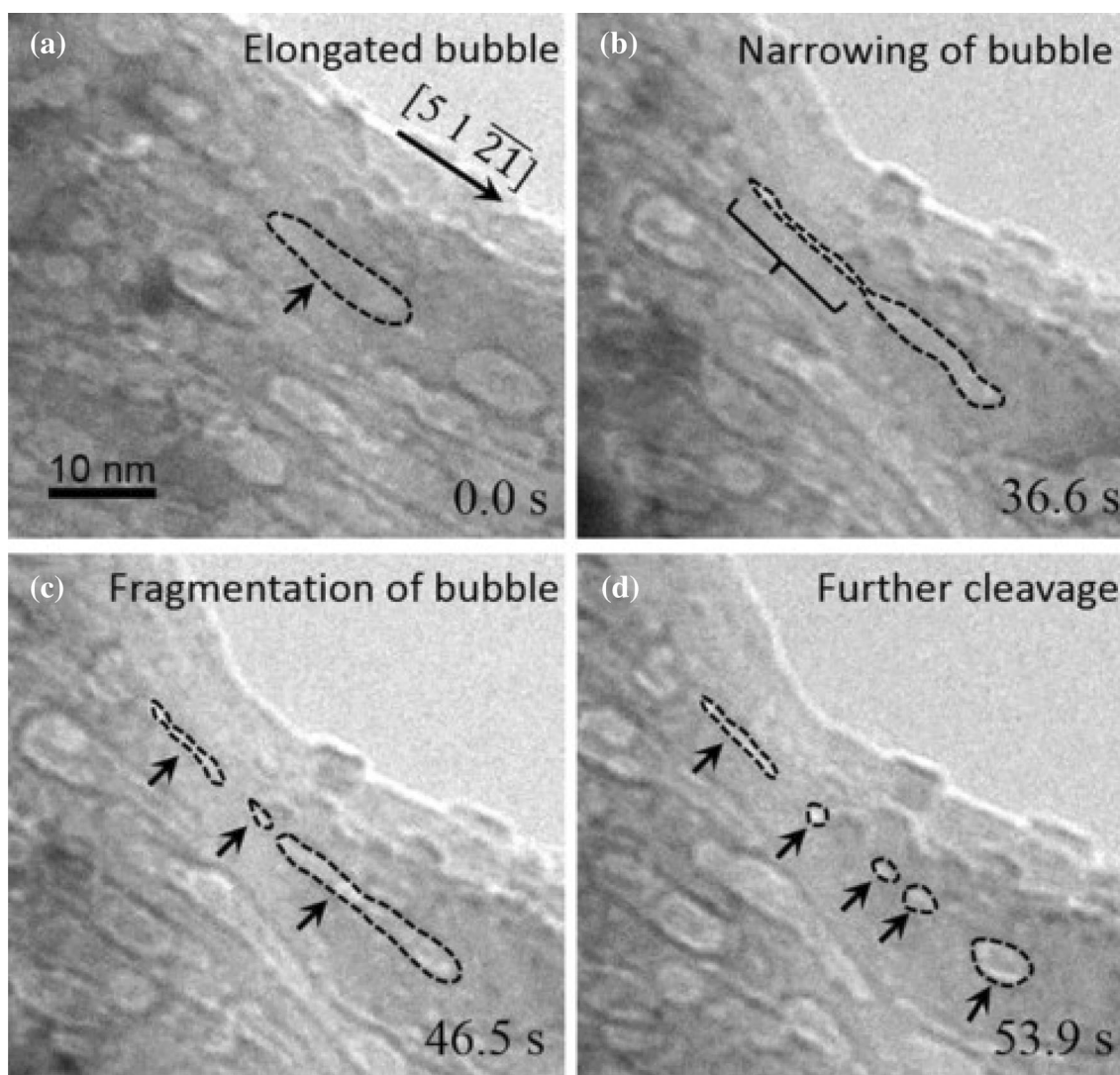


Fig. 5. Fragmentation of a helium bubble into several tiny bubbles during severe straining (reprinted with permission from Ref. 12). (a) Slightly elongated bubbles after stretch; (b) left part of the bubble shrunk down to ~ 1 nm in width with further deformation; (c) the severely elongated bubble fragmented into three segments; (d) further fragmentation of the stretched bubbles into five tiny bubbles.

produce deformation twins in helium-irradiated Cu.⁵⁹ The interactions between these Shockley partials and helium bubbles induce hardening during twinning. Notably, the back stresses generated by dislocation–bubble interactions elicit partial detwinning of the deformation twins. The accumulated back stress-induced detwinning is also observed in other metals.^{60–62} Figure 6 demonstrates the processes of twinning and detwinning in helium-bubbled (NB) Cu pillars under strain.⁵⁹ The NB-Cu pillar has a growth twin with its twin boundaries almost perpendicular to the loading axis. Upon loading, the sample yields at a stress of 0.75 GPa. The nucleation of twins induces a sudden strain jump, as marked in the stress–strain curve in Fig. 6k. With further straining, two new twins (T2, T3) nucleated and grew sluggishly during tension (Fig. 6c–e). With the assistance of accumulated back stress, partial detwinning took place at a lower

stress when the strains were relaxed due to fracture or when the loading direction was reversed (Fig. 6f–k). Furthermore, the twinning stress exhibited asymmetry in tension and compression during cyclic loading due to the accumulated back stress produced by dislocation–bubble interactions.⁵⁹

Failure Induced by Helium Bubble Coalescence and Fragmentation

Strain localization dramatically accelerates the coarsening and coalescence of helium bubbles, which causes the final failure of the samples.^{10,15} Figure 7 demonstrates the morphology of a fracture surface in micro-scale Zr tensile samples with and without helium bubbles (HB-Zr and FD-Zr).¹³ Compared with the cleavage fracture surface of FD-Zr, HB-Zr shows a fracture surface with many connected holes, indicating that the bubbles coalesce in the final stage of failure (Fig. 7).¹³ Furthermore,

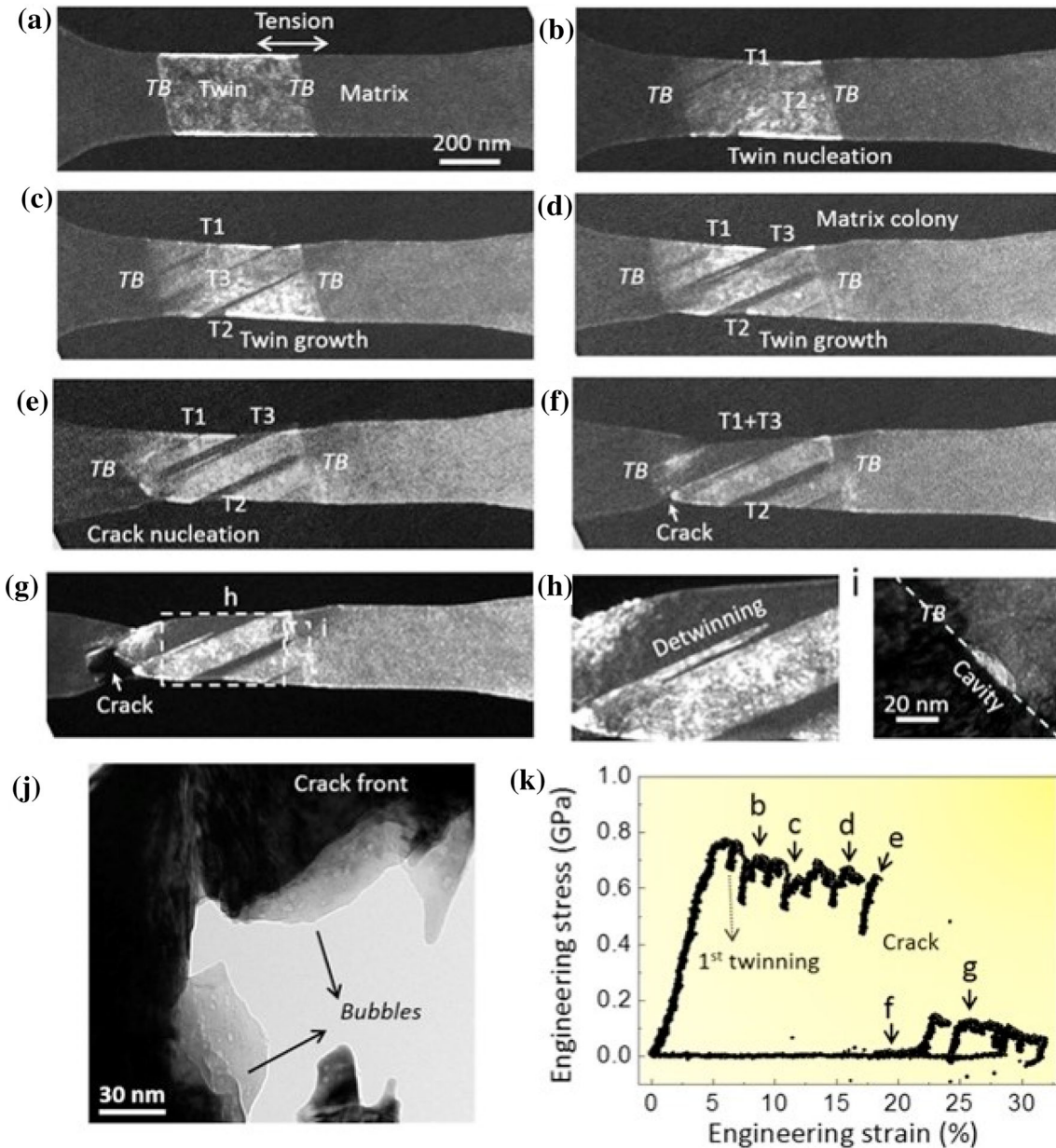


Fig. 6. In situ tensile deformation of a growth twin embedded helium-irradiated Cu sample (reprinted with permission from Ref. 59). (a) Dark field TEM image showing the growth twin in the tensile sample; (b) secondary twins nucleate inside the growth twin on loading; (c) more deformation twins nucleate from the sample edges in the growth twin, with straining; (d) deformation twins interact with the boundaries of growth twin; (e) stress concentration develops at the deformation twin-growth twin boundary interface; (f) crack nucleates from the stress concentration; (g) partial detwinning of deformation twin occurs due to crack formation-induced strain relaxation; (h) magnified image of partially detwinned region in (g); (i) magnified image of a cavity nucleated at the growth twin boundary–deformation twin interface, on unloading; (j) enlarged helium bubbles seen at the fracture surface, indicating their coalescence; (k) engineering stress strain curve of the tensile test (points marked on the curve with black arrows correspond to the image labels (b–g)).

due to the preferential growth of helium bubbles along the basal plane, HB-Zr with the basal plane on the maximum shear stress orientation displays a near cleavage fracture, while FD-Zr with a similar orientation shows a curved fracture front, which indicates that the bubble coalescence in the basal plane induced the final failure (Fig. 7c and d).¹³

Bubble coalescence is also widely observed in regions with high localized strain. In situ experiments demonstrated that spacing of bubbles

distributed in localized deformation regions reduce with increasing strain, giving rise to coalescence of adjacent bubbles.^{10,15} A transition from large helium bubbles to cavities occur with the aid of bubble coalescence and further coarsening by absorbing plasticity-induced vacancies.¹⁵ Finally, cavity coarsening, coalescence, and link-up lead to fracture in the samples.^{11,12,15} Figure 8 shows the bubble coalescence-induced crack propagation in helium-irradiated Cu cantilever during loading.

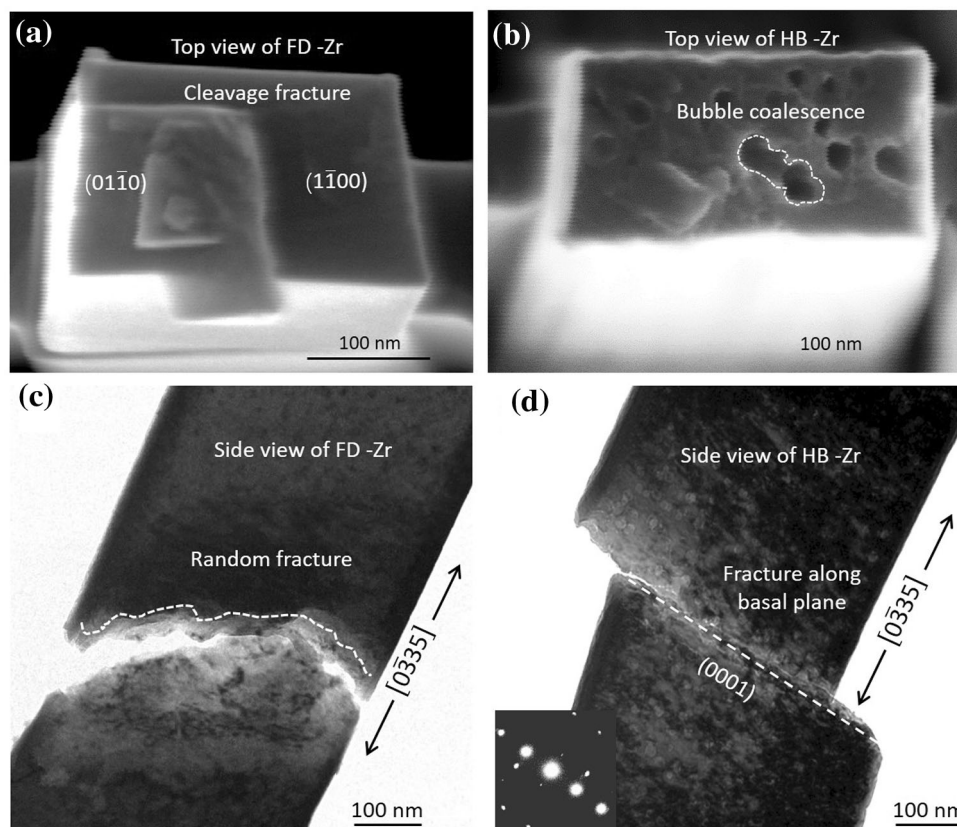


Fig. 7. The morphology of the fracture surface of Zr samples with helium bubbles (HB-Zr) and without helium bubbles (FD-Zr) (reprinted with permission from Ref. 13). (a) SEM image of Zr single crystal shows a cleavage fracture surface along the prismatic plane; (b) SEM image of helium-bubbled Zr showing bubble coalescence-induced fracture; (c) TEM image of fully dense Zr with basal plane on the maximum shear stress plane showing a curve fracture front; (d) TEM image of helium-bubbled Zr with basal plane on the maximum shear stress plane showing a near-cleavage fracture along the basal.

With tearing, partial dislocations begin to operate in the front of the notch (Fig. 8b).¹⁵ With further deformation, several helium bubbles at the notch tip begin to grow. Subsequently, some of the helium bubbles located along the sample-thickness direction underwent coalescence to form cavities and holes (Fig. 8c), then the connection of multiple cavities/holes led to crack propagation (Fig. 8d, e).¹⁵ During the growth and propagation of the internal cracks, the walls between the helium bubbles developed into nano-bridges.¹⁵ This bridging is a mechanism to delay the crack propagation in NB-Cu.^{59,63}

Besides the bubble coalescence, bubble fragmentation is another novel micro-damaging mechanism in helium-irradiated metals. Bubble fragmentation is mediated by the combination of dislocation cutting and internal surface diffusion, which is an alternative micro-damaging mechanism in helium-irradiated copper in addition to the bubble coalescence.¹² Some of the bubbles were severely elongated once necking started (Fig. 5). With further tensile deformation, some bubbles rapidly narrowed and evolved into a long rod-like bubble, while other

bubbles were only slightly elongated due to the inhomogeneous local strain.¹² Further deformation split the long rod-like bubbles into three segments (Fig. 5c). In the subsequent straining, the deformation was localized in the right section of the helium bubble and led to a severe reduction of the bubble width, which finally split into three parts (Fig. 5d). A similar bubble fragmentation has also been observed around the fracture tip in other metals.⁶⁴ Rows of bubbles were formed due to the extreme elongation of bubbles under stress and their subsequent division into smaller pieces.⁶⁴ The bubble rows tend to form in parallel to the slip direction in metals.⁶⁴ The fragmentation of helium bubbles causes the alignment of splitting bubbles along a shear-deformation zone, which promotes the formation of a bubble-free channel and thus accelerates strain localization and failure in helium-irradiated metals.^{12,45} The role of a helium bubble-free channel is similar to the defect-free channels frequently observed in irradiated metals,^{65–67} which cause the previously mentioned failure of structural components in nuclear reactors.

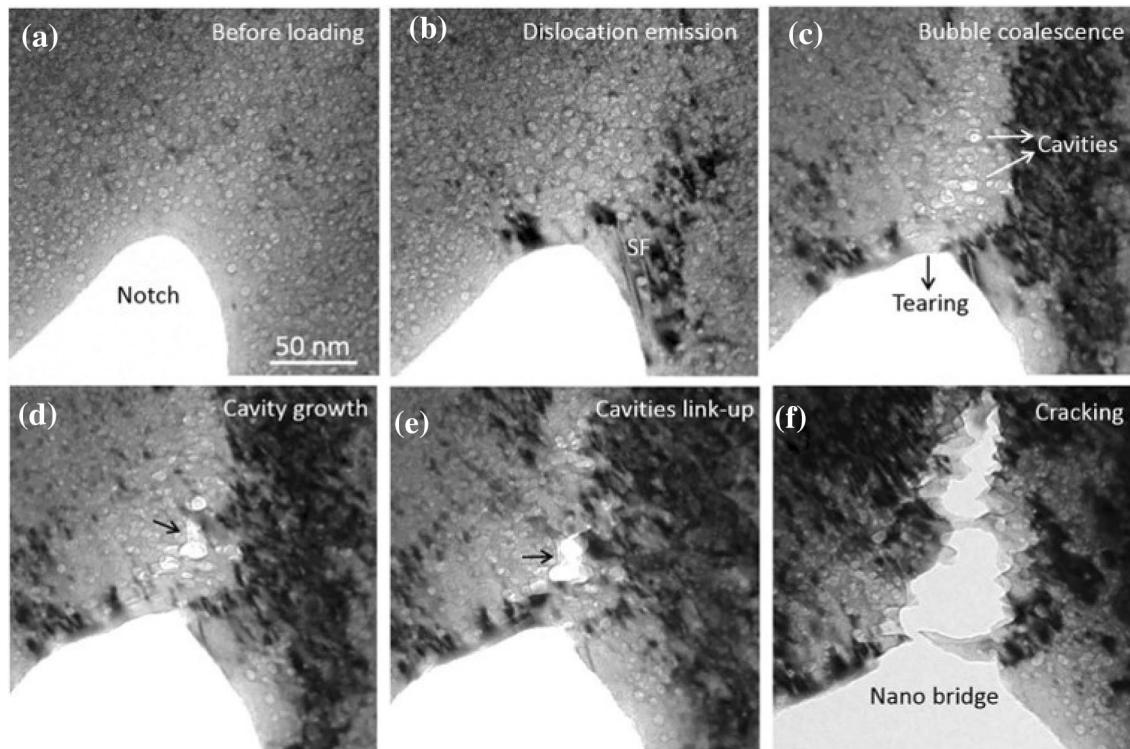


Fig. 8. Images of the cracking behavior of a Cu single-crystal cantilever sample with high density of helium bubbles and loading along [100] (reprinted with permission from Ref. 15). (a) The microstructure of the helium bubbles at the front of the notch prior to loading; (b) partial dislocation emissions, leading to the formation of stacking faults (SFs) at the notched area; (c) coalescence of helium bubbles along the sample-thickness direction, triggering the formation of large holes/cavities; (d) further in-plane bubble coalescences promote the growth of cavities; (e) crack nucleation via the link-up of isolated cavities; (f) nano-bridge formation during crack propagation.

SUMMARY AND OUTLOOK

In this review, we briefly summarized the previous studies on in situ observation of the dynamics of helium bubbles under thermal annealing, irradiation, and mechanical loading. Upon annealing, helium bubbles show a Brownian motion either in grains or along the grain boundaries. The diffusivity of the bubbles depends on the adjacent chemical composition, bubble size, bubble shape, and annealing temperature. OR and MC are the mechanisms for bubble growth and coarsening. Under in situ irradiation, helium bubbles undergo migration, coalescence, coarsening, and shrinkage, which are mediated by cascade-induced thermal spikes and radiation defects. Helium bubbles show migration, coarsening, elongation, and cleavage under mechanical loading. Helium bubbles migrate because of the stress gradient. Dislocation cutting and internal surface diffusion also assist the dynamic evolution of helium bubbles under strain. Bubble–dislocation interactions and bubble–twin interactions could dramatically alter the deformation mode of metals and alloys. During deformation, helium bubbles play the combined role of shearable obstacles and internal dislocation sources, which enhance strength and improve deformability. Bubble

coalescence and fragmentation are micro-damaging mechanisms inducing the final failure of helium-irradiated metals.

As typical radiation-induced defects, helium bubbles demonstrate diverse evolutionary dynamics under stimulation. However, some opportunities or challenges remain in understanding the role of helium bubbles in metals. First, face-centered cubic (FCC) metals are simple model materials for studying the dynamic evolution of helium bubbles. Nonetheless, the dynamic behavior of helium bubbles in hexagonal close-packed (HCP) and body-centered cubic (BCC) metals is of concern in practice. Therefore, revealing the dynamic deformation behavior of BCC and HCP metals containing helium bubbles by in situ tools should be the next step. Second, bi-metal interfaces are well-known efficient sinks for radiation-induced defects, which have attracted great interest in recent decades. Although helium bubbles were observed with Brownian motion along the grain boundary in FCC metals, the details of the interaction between helium bubbles and phase interface are lacking. Third, the spatiotemporal resolution of imaging under in situ stimulations needs to be improved to capture more details of the dynamic evolution of helium bubbles.

ACKNOWLEDGEMENTS

This work was supported by the National Natural Science Foundation of China (Grant Nos. 51922082, 51971170 and 51942104), the National Key Research and Development Program of China (2017YFB0702301), the 111 Project of China (Grant Number BP2018008) and the Innovation Project of Shaanxi Province (Grant No. 2017KTPT-12).

CONFLICT OF INTEREST

The authors declare no conflict of interest.

REFERENCES

- J. Laakmann, P. Jing, and W. Uelhoff, *Acta Metall.* 35, 2063 (1987).
- H. Ullmaier, *Radiat. Eff.* 78, 1 (2006).
- V.N. Chernikov, H. Trinkaus, P. Jung, and H. Ullmaier, *J. Nucl. Mater.* 170, 31 (1990).
- K. Yutani, H. Kishimoto, R. Kasada, and A. Kimura, *J. Nucl. Mater.* 367, 423 (2007).
- S.J. Zinkle and G.S. Was, *Acta Mater.* 61, 735 (2013).
- R. Bès, C. Gaillard, N. Millard-Pinard, S. Gavarini, P. Martin, S. Cardinal, C. Esnouf, A. Malchère, and A. Perrat-Mabilon, *J. Nucl. Mater.* 434, 56 (2013).
- H. Trinkaus and B.N. Singh, *J. Nucl. Mater.* 323, 229 (2003).
- T. Yamamoto, G.R. Odette, H. Kishimoto, J.W. Rensman, and P. Miao, *J. Nucl. Mater.* 356, 27 (2006).
- H.F. Huang, W. Zhang, M. De Los Reyes, X.L. Zhou, C. Yang, R. Xie, X.T. Zhou, P. Huai, and H.J. Xu, *Mater. Des.* 90, 359 (2016).
- M.S. Ding, J.P. Du, L. Wan, S. Ogata, L. Tian, E. Ma, W.Z. Han, J. Li, and Z.W. Shan, *Nano Lett.* 16, 4118 (2016).
- S.H. Li, J. Zhang, and W.Z. Han, *Scr. Mater.* 165, 112 (2019).
- M.S. Ding, L. Tian, W.Z. Han, J. Li, E. Ma, and Z.W. Shan, *Phys. Rev. Lett.* 117, 215501 (2016).
- S.M. Liu, S.H. Li, and W.Z. Han, *J. Mater. Sci. Technol.* 35, 1466 (2019).
- S.H. Li, W.Z. Han, and Z.W. Shan, *Acta Mater.* 141, 183 (2017).
- W.Z. Han, M.S. Ding, and Z.W. Shan, *Scr. Mater.* 147, 1 (2018).
- A. Reichardt, M. Ionescu, J. Davis, L. Edwards, R.P. Harrison, P. Hosemann, and D. Bhattacharyya, *Acta Mater.* 100, 147 (2015).
- Y.T. Ma, J.B. Liu, L. Han, L.F. Tian, X.C. Wang, X.M. Meng, S.Q. Xiao, and B. Wang, *Acta Phys. Sin.* 68, 040702 (2019).
- J. Gao, H. Huang, J. Liu, J. Zeng, R. Xie, and Y. Li, *Scr. Mater.* 158, 121 (2019).
- N.R. Catarineu, N.C. Bartelt, J.D. Sugar, S.M. Vitale, K.L. Shanahan, and D.B. Robinson, *J. Phys. Chem. C* 123, 19142 (2019).
- K. Hojou, H. Otsu, S. Furuno, K. Izui, and T. Tsukamoto, *J. Nucl. Mater.* 212, 281 (1994).
- K. Ono, S. Furuno, K. Hojou, T. Kino, K. Izui, O. Takaoka, N. Kubo, K. Mizuno, and K. Ito, *J. Nucl. Mater.* 191, 1269 (1992).
- K. Ono, S. Furuno, S. Kanamitsu, and K. Hojou, *Philos. Mag. Lett.* 75, 59 (1997).
- K. Ono, K. Arakawa, M. Oohashi, H. Kurata, K. Hojou, and N. Yoshida, *J. Nucl. Mater.* 283, 210 (2000).
- K. Ono, K. Arakawa, K. Hojou, M. Oohashi, R. Birtcher, and S. Donnelly, *J. Electron Microsc.* 51, 5245 (2002).
- K. Ono, K. Arakawa, and K. Hojou, *J. Nucl. Mater.* 307, 1507 (2002).
- H. Zhang, F. Ren, Y. Wang, M. Hong, X. Xiao, W. Qin, and C. Jiang, *J. Nucl. Mater.* 467, 537 (2015).
- Q. Wei, N. Li, K. Sun, and L.M. Wang, *Scr. Mater.* 63, 430 (2010).
- J. Gao, H. Huang, X. Liu, C. Wang, J.F. Stubbins, and Y. Li, *Scr. Mater.* 147, 93 (2018).
- K. Ono, M. Miyamoto, H. Kurata, M. Haruta, and A. Yatommi, *J. Appl. Phys.* 126, 135104 (2019).
- K. Ono, M. Miyamoto, K. Arakawa, and R.C. Birtcher, *Philos. Mag.* 89, 513 (2009).
- N. Marochov, L.J. Perryman, and P.J. Goodhew, *J. Nucl. Mater.* 149, 296 (1987).
- P.J. Goodhew and D.K. Tyler, *Proc. R. Soc. Lond. A* 377, 151 (1981).
- B.N. Singh and H. Trinkaus, *J. Nucl. Mater.* 186, 153 (1992).
- A.J. Markworth, *Metall. Trans. A* 4, 2651 (1973).
- M.A. Van Huis, A. Van Veen, F. Labohm, A.V. Fedorov, H. Schut, B.J. Kooi, and J.T.M. De Hosson, *Nucl. Instrum. Methods B* 216, 149 (2004).
- P.J. Goodhew, *J. Nucl. Mater.* 98, 221 (1981).
- H. Schroeder and P.F.P. Fichtner, *J. Nucl. Mater.* 179, 1007 (1991).
- H.H. Shen, S.M. Peng, B. Chen, F.N. Naab, G.A. Sun, W. Zhou, X. Xiang, K. Sun, and X.T. Zu, *Mater. Charact.* 107, 309 (2015).
- K. Ono, K. Arakawa, and R.C. Birtcher, *Nucl. Instrum. Methods B* 206, 14 (2003).
- K. Ono, M. Miyamoto, K. Arakawa, and R.C. Birtcher, *Nucl. Instrum. Methods B* 242, 455 (2006).
- M. Miyamoto, K. Ono, K. Arakawa, and R.C. Birtcher, *J. Nucl. Mater.* 367, 350 (2007).
- S.E. Donnelly, R.C. Birtcher, C. Tehplier, R. Valizadeh, V. Vishnyakov, Presented at the Materials Research Society (MRS) 1994 Fall Meeting, November 28–December 2, 1994, Boston, MA (1994).
- R.C. Birtcher, S.E. Donnelly, and C. Templier, *Phys. Rev. B* 50, 764 (1994).
- M.F. Beaufort, M. Vallet, J. Nicolai, E. Oliviero, and J.F. Barbot, *J. Appl. Phys.* 118, 205904 (2015).
- W. Beeré, *Scr. Metall.* 9, 999 (1975).
- E. Ruedl and P. Schiller, *J. Nucl. Mater.* 85, 769 (1979).
- H. Chen, Y. Cheng, C. Lin, J. Peng, X. Liang, J. Gao, W. Liu, and H. Huang, *J. Nucl. Mater.* 520, 178 (2019).
- H. Chen, W. Liu, Y. Cheng, J. Peng, X. Liang, L. Hu, and G. Wang, *Mater. Lett.* 247, 11 (2019).
- S.H. Li, J.T. Li, and W.Z. Han, *Materials* 12, 1036 (2019).
- A. Singh, S. Maji, and P.M.G. Nambissan, *J. Phys. Condens. Matter* 13, 177 (2001).
- S.M. Hafez Haghghat and R. Schäublin, *Philos. Mag.* 90, 1075 (2010).
- R.N. Wright and C. Dew Van Sicle, *J. Nucl. Mater.* 206, 87 (1993).
- Z.J. Wang, F.I. Allen, Z.W. Shan, and P. Hosemann, *Acta Mater.* 121, 78 (2016).
- Q. Guo, P. Landau, P. Hosemann, Y. Wang, and J.R. Greer, *Small* 9, 691 (2013).
- R. Lontas, X.W. Gu, E. Fu, Y. Wang, N. Li, N. Mara, and J.R. Greer, *Nano Lett.* 14, 5176 (2014).
- W.Z. Han, J. Zhang, M.S. Ding, L. Lv, W.H. Wang, G.H. Wu, Z.W. Shan, and J. Li, *Nano Lett.* 17, 3725 (2017).
- C. Bewerse, L.C. Brinson, and D.C. Dunand, *Acta Mater.* 115, 83 (2016).
- M. Chmielus, X.X. Zhang, C. Witherspoon, D.C. Dunand, and P. Mullner, *Nat. Mater.* 8, 863 (2009).
- W.Z. Han, M.S. Ding, R.L. Narayan, and Z.W. Shan, *Adv. Eng. Mater.* 19, 1700357 (2017).
- M. Arul-Kumar, A.K. Kanjarla, S.R. Niezgodna, R.A. Lebensohn, and C.N. Tomé, *Acta Mater.* 84, 349 (2015).
- D. Shi, T. Liu, L. Zhang, D. Hou, H. Chen, F. Pan, and L. Lu, *Mater. Sci. Eng. A* 667, 132 (2016).
- S.J. McCormack, W. Wen, E.V. Pereloma, C.N. Tome, A.A. Gazder, and A.A. Saleh, *Acta Mater.* 156, 172 (2018).
- A. Pineau, A.A. Benzerga, and T. Pardoen, *Acta Mater.* 107, 424 (2016).
- K. Arakawa, K. Ono, H. Tanigawa, Y. Katoh, A. Kohyama, and M. Kiritani, *Mater. Sci. Eng. A* 350, 53 (2003).
- Y. Dai and M. Victoria, *MRS Symp. Proc.* 439, 319 (1997).

66. T.D. de la Rubia, H.M. Zbib, T.A. Khraishi, B.D. Wirth, M. Victoria, and M.J. Caturla, *Nature* 406, 871 (2000).
67. Y. Fan, Y.N. Osetskiy, S. Yip, and B. Yildiz, *Proc. Natl. Acad. Sci. USA* 110, 17756 (2013).

Publisher's Note Springer Nature remains neutral with regard to jurisdictional claims in published maps and institutional affiliations.